Mixel camera—a new push-broom camera concept for high spatial resolution keystone-free hyperspectral imaging

Gudrun Høye[1,3] and Andrei Fridman[2,*]

[1]*Norwegian Defence Research Establishment (FFI), P O Box 25, 2027 Kjeller, Norway*
[2]*Norsk Elektro Optikk, P O Box 384, 1471 Lørenskog, Norway*
[3]*Gudrun-Kristine.Hoye@ffi.no*
[*]*fridman@neo.no*

Abstract: Current high-resolution push-broom hyperspectral cameras introduce keystone errors to the captured data. Efforts to correct these errors in hardware severely limit the optical design, in particular with respect to light throughput and spatial resolution, while at the same time the residual keystone often remains large. The mixel camera solves this problem by combining a hardware component – an array of light mixing chambers – with a mathematical method that restores the hyperspectral data to its keystone-free form, based on the data that was recorded onto the sensor with large keystone. A Virtual Camera software, that was developed specifically for this purpose, was used to compare the performance of the mixel camera to traditional cameras that correct keystone in hardware. The mixel camera can collect at least four times more light than most current high-resolution hyperspectral cameras, and simulations have shown that the mixel camera will be photon-noise limited – even in bright light – with a significantly improved signal-to-noise ratio compared to traditional cameras. A prototype has been built and is being tested.

OCIS codes: (110.4234) Multispectral and hyperspectral imaging; (120.0280) Remote sensing and sensors; (120.6200) Spectrometers and spectroscopic instrumentation; (220.4830) Systems design; (300.6190) Spectrometers; (100.3190) Inverse problems.

References and links

1. P. Mouroulis, R. O. Green, and T. G. Chrien, "Design of pushbroom imaging spectrometers for optimum recovery of spectroscopic and spatial information," Appl. Opt. **39**(13), 2210–2220 (2000).
2. P. Mouroulis, B. E. Van Gorp, V. E. White, J. M. Mumolo, D. Hebert, and M. Feldman, "A compact, fast, wide-field imaging spectrometer system," Proc. SPIE **8032**, 80320U, 80320U-12 (2011).
3. P. Mouroulis, B. Van Gorp, R. O. Green, M. Eastwood, J. Boardman, B. S. Richardson, J. I. Rodriguez, E. Urquiza, B. D. Franklin, and B. C. Gao, "Portable remote imaging spectrometer (PRISM): laboratory and field calibrations," Proc. SPIE **8515**, 85150F, 85150F-10 (2012).
4. P. Mouroulis, R. O. Green, and D. W. Wilson, "Optical design of a coastal ocean imaging spectrometer," Opt. Express **16**(12), 9087–9096 (2008).
5. G. Høye and A. Fridman, "Hyperspektralt kamera og metode for å ta opp hyperspektrale data," Norwegian patent application number 20111001.
6. G. Høye and A. Fridman, "Hyperspectral camera and method for acquiring hyperspectral data," PCT international patent application number PCT/NO2012/050132.
7. G. Høye and A. Fridman, "A method for restoring data in a hyperspectral imaging system with large keystone without loss of spatial resolution," FFI-rapport 2009/01351 (2009), declassified on January 28th 2013.
8. A. Fridman, G. Høye, and T. Løke, "Resampling in hyperspectral cameras as an alternative to correcting keystone in hardware, with focus on benefits for the optical design and data quality," Proc. SPIE (to be published).
9. M. Traub, H. D. Hoffmann, H. D. Plum, K. Wieching, P. Loosen, and R. Poprawe, "Homogenization of high power diode laser beams for pumping and direct applications," Proc. SPIE **6104**, 61040Q, 61040Q-10 (2006).
10. H. Guckel, "High-aspect-ratio micromachining via deep X-ray lithography," Proc. IEEE **86**(8), 1586–1593 (1998).
11. P. Mouroulis and R. O. Green, "Optical design for high fidelity imaging spectrometry," Proc. SPIE **4829**, 1048–1049 (2003).
12. http://www.hyspex.no/products/hyspex/vnir1600.php

#185751 - $15.00 USD Received 21 Feb 2013; revised 22 Apr 2013; accepted 23 Apr 2013; published 29 Apr 2013

13. R. Lucke and J. Fisher, "The Schmidt-Dyson: a fast space-borne wide-field hyperspectral imager," Proc. SPIE **7812**, 78120M, 78120M-13 (2010).
14. G. Høye and A. Fridman, "Performance analysis of the proposed new restoring camera for hyperspectral imaging," FFI-rapport 2010/02383 (2010), to be declassified.
15. Technical specifications on CIS 2521F (last accessed 20.04.2013), *http://www.fairchildimaging.com/catalog/focal-plane-arrays/scmos/cis-2521f*
16. B. E. A. Salech and M. C. Teich, *Fundamentals of Photonics* (John Wiley & Sons Inc., 1991).

1. Introduction

Hyperspectral cameras are increasingly used for various military, scientific, and commercial purposes. Push-broom cameras are particularly popular when high spatial and spectral resolution in combination with high signal-to-noise ratio is required. Figure 1 shows the principle of operation of a push-broom hyperspectral camera. Unfortunately, these cameras also introduce spatial and spectral artefacts, known as keystone and smile, to the recorded hyperspectral data [1]. This may significantly distort the captured spectra, see Fig. 2.

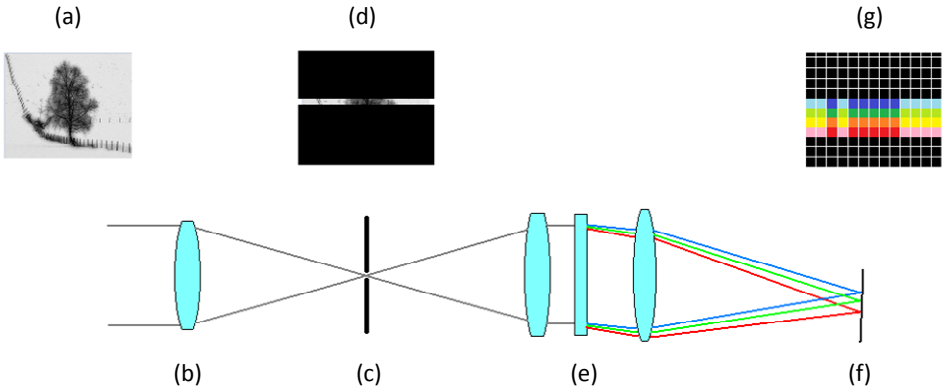

Fig. 1. Light from the scene (a) is focused by the foreoptics (b) onto the slit plane (c). The slit blocks most of the scene, leaving only a narrow horizontal portion (d) of the scene visible. The relay optics (e) forms an image of the scene with superimposed slit onto the sensor (f). Because of the presence of a dispersive element in the relay optics, each point of the narrow horizontal line (d) is stretched (dispersed) in the vertical direction. The image on the sensor (g) contains spectra for each small area of the scene (d). A 2-dimensional image is obtained by scanning in the vertical direction.

Users would like to have cameras with high resolution, high sensitivity, and at the same time very low smile and keystone errors. The requirements for smile and keystone are normally set to a fraction of a pixel, and hyperspectral cameras therefore have extremely tight tolerances for optical aberrations compared to other imaging systems where corrections are required only at pixel level. As a result, the development of hyperspectral cameras has more or less converged to a couple of standard layouts, each of them with some inherent limitations such as minimum possible F-number, maximum possible spatial resolution, etc.

As new sensors with higher pixel count become available, camera manufacturers try to develop the optics for these sensors. This optics must be sharper and faster in order to justify the use of a newer, better sensor. And since the requirements for smile and keystone are set relative to the pixel size, the absolute smile and keystone errors must decrease. This makes the development of new optics increasingly difficult.

#185751 - $15.00 USD Received 21 Feb 2013; revised 22 Apr 2013; accepted 23 Apr 2013; published 29 Apr 2013

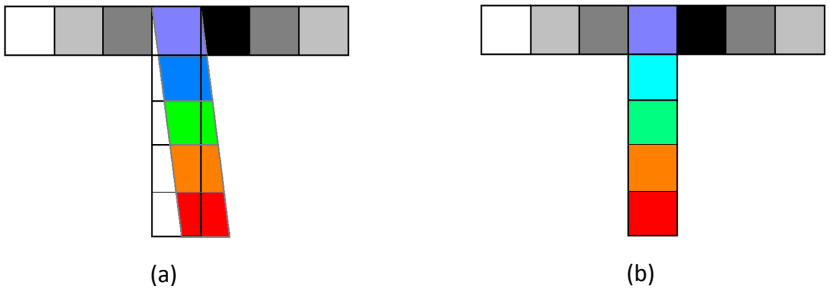

Fig. 2. The light from a small scene area is dispersed in the vertical direction, creating an image of the spectrum in the sensor plane. When the keystone is large (a), some wavelengths (particularly red, in this example) are partially projected onto the neighboring pixels on the sensor. As a result, the spectrum, captured by one column of sensor pixels, may contain large errors. A perfect keystone-free optics would project the same spectrum onto the sensor as shown in (b). Then, the captured spectrum would be correct.

Smile could be handled by oversampling the spectrum, since typically there are significantly more pixels on the sensor in the spectral direction than the required number of spectral channels. However, in the spatial direction one normally wants to take advantage of the full resolution of the sensor and resolve with reasonably good contrast pixel sized details. Therefore the problem with keystone cannot be handled the same way.

Some of the recent designs [2–4] have good light gathering capacity and an impressive level of keystone correction (0.05 pixel and less), when used with a ~640 pixels sensor. The latest sensors may have up to 10 000 pixels in the spatial direction. Making cameras based on these sensors with a requirement of having the keystone typically less than 0.1 pixel, means correcting lateral chromatic aberration and distortion in such cameras as precise as a fraction 0.00002 of the image size. Probably, the word “challenging” does not quite describe the difficulty of this task.

But is it really necessary to have so tight requirements for the keystone? All the data is still there, even when large keystone is present in the system, it is just not arranged in the same “neat” way on the sensor. Could it be possible to restore the data to its preferred keystone-free form (Fig. 3) based on the data recorded on the sensor with large keystone?

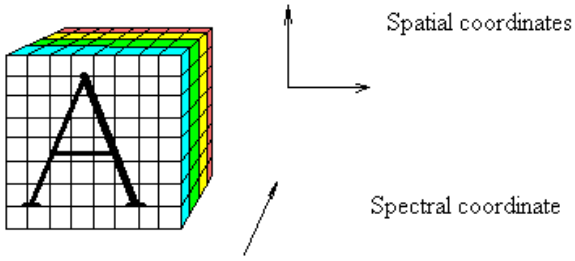

Fig. 3. Datacube. Hyperspectral data should preferably be completely keystone-free so that the spectral information for each spatial pixel is correct.

The mixel camera presented in this article, is able to do this in a lossless way by combining a hardware component (an array of light mixing chambers that is inserted into the camera slit) and a mathematical method to restore the data. The mathematical method is explained in Section 2 and the light mixing chambers are described in Section 3. Lifting the stringent requirements to keystone correction makes the optical design task very much easier and opens up for the possibility to design hyperspectral cameras that can collect at least four times more light than the widely used Offner design, as we will show in Section 4. In order to compare the performance of the mixel camera to traditional hyperspectral cameras, a Virtual Camera software was developed and is described in Section 5. The performance of the mixel camera is then compared to the performance of traditional cameras in Section 6. The mixel

#185751 - $15.00 USD Received 21 Feb 2013; revised 22 Apr 2013; accepted 23 Apr 2013; published 29 Apr 2013

camera requires very precise knowledge about the relative position between the sensor pixels and the array of light mixing chambers, and a method for precise camera calibration is suggested in Section 7. Finally, a conclusion is given in Section 8.

Norwegian and international PCT patent applications have been filed for the technology presented in this article [5,6]. A hyperspectral camera prototype according to the proposed concept has been built and is currently being tested.

2. The data restoring method

We will explain the method for restoring the data to keystone-free form by a simple numerical example. Consider one spatial line which is 4 pixels long and assume that at a certain wavelength there is 1 pixel keystone. The 4 pixels from the scene are then recorded into 5 pixels on the sensor, see Fig. 4(a). Assume that in case of this particular scene at this particular wavelength the pixels in the scene have the following values (i.e., energies): E_1 = 10, E_2 = 30, E_3 = 100, and E_4 = 50. This gives the following values E^R for the recorded sensor pixels:

$$\begin{aligned} E_1^R &= \tfrac{4}{5}\cdot E_1 = \tfrac{4}{5}\cdot 10 = 8, \\ E_2^R &= \tfrac{1}{5}\cdot E_1 + \tfrac{3}{5}\cdot E_2 = \tfrac{1}{5}\cdot 10 + \tfrac{3}{5}\cdot 30 = 20, \\ E_3^R &= \tfrac{2}{5}\cdot E_2 + \tfrac{2}{5}\cdot E_3 = \tfrac{2}{5}\cdot 30 + \tfrac{2}{5}\cdot 100 = 52, \\ E_4^R &= \tfrac{3}{5}\cdot E_3 + \tfrac{1}{5}\cdot E_4 = \tfrac{3}{5}\cdot 100 + \tfrac{1}{5}\cdot 50 = 70, \\ E_5^R &= \tfrac{4}{5}\cdot E_4 = \tfrac{4}{5}\cdot 50 = 40, \end{aligned} \tag{1}$$

when we assume that the intensity distribution over each pixel in the scene is uniform. In a real scene this will not be the case, but we will show how this can be handled in Section 3.

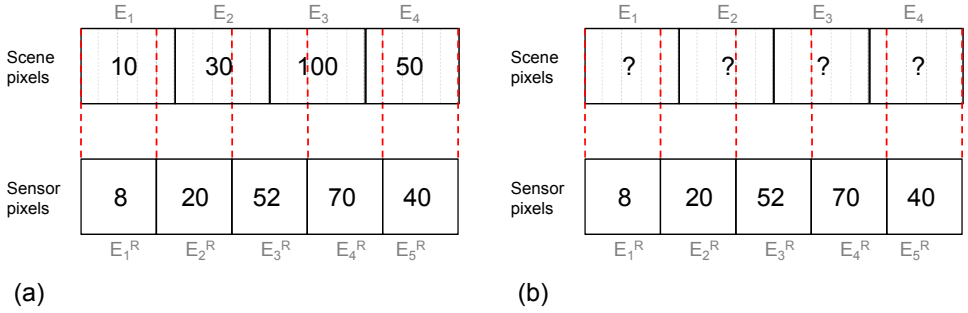

Fig. 4. The figure shows (a) scene pixels with known values and corresponding recorded sensor pixels, and (b) recorded sensor pixels with known values and corresponding scene pixels with unknown values.

In reality, we will not know the actual values of the scene pixels, and this situation is shown in Fig. 4(b). In order to determine the values of the scene pixels, we set up the following set of equations:

$$\begin{aligned} \tfrac{4}{5}\cdot E_1 &= E_1^R = 8, \\ \tfrac{1}{5}\cdot E_1 + \tfrac{3}{5}\cdot E_2 &= E_2^R = 20, \\ \tfrac{2}{5}\cdot E_2 + \tfrac{2}{5}\cdot E_3 &= E_3^R = 52, \\ \tfrac{3}{5}\cdot E_3 + \tfrac{1}{5}\cdot E_4 &= E_4^R = 70, \\ \tfrac{4}{5}\cdot E_4 &= E_5^R = 40. \end{aligned} \tag{2}$$

The equation system (2) can easily be solved for the unknown scene pixel values E_1, E_2, E_3, and E_4, giving the following values: E_1 = 10, E_2 = 30, E_3 = 100, and E_4 = 50, which are

#185751 - $15.00 USD Received 21 Feb 2013; revised 22 Apr 2013; accepted 23 Apr 2013; published 29 Apr 2013

identical to the actual values in the scene pixels as given in Fig. 4(a). We have now managed to restore the true values of the 4 pixels in the scene, based only on the information about the values of the 5 recorded sensor pixels and the amount of keystone (1 pixel). In addition, we have assumed that the light distribution is uniform within each scene pixel, but as we will see below, it is sufficient that the light distribution is known (not necessarily uniform).

Let us now consider the general situation where we want to restore N pixels in the scene from M recorded sensor pixels, where $M>N$. This situation is shown in Fig. 5.

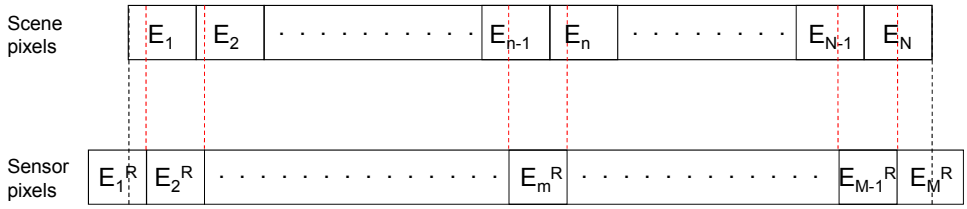

Fig. 5. Scene pixels and corresponding recorded sensor pixels for the general case.

We can now set up the following set of general equations:

$$E^R_m = \sum_{n=1}^{N} q_{mn} E_n, \qquad m = 1,2,...,m,...,M-1,M, \tag{3}$$

where E_n is the pixel value (energy) for scene pixel #n, E^R_m is the pixel value (energy) recorded in sensor pixel #m, q_{mn} is the fraction of the energy contained within scene pixel #n that contributes to the value (energy) recorded in sensor pixel #m, N is the total number of pixels in the scene, and M is the total number of pixels recorded on the sensor.

The matrix coefficients q_{mn} depend on the keystone and point-spread function (see Section 6.4) of the system, and are measured during camera calibration/characterization. Typically, only two scene pixels contribute to each recorded sensor pixel, therefore most of the coefficients q_{mn} are equal to zero. Equation (3) can then be written in matrix form:

$$\begin{pmatrix} q_{11} & & & & & & \\ q_{21} & q_{22} & & & & & \\ & \ddots & \ddots & & & & \\ & & q_{m(n-1)} & q_{mn} & & & \\ & & & \ddots & \ddots & & \\ & & & & q_{(M-1)(N-1)} & q_{(M-1)N} & \\ & & & & & q_{MN} \end{pmatrix} \cdot \begin{pmatrix} E_1 \\ \vdots \\ E_n \\ \vdots \\ E_N \end{pmatrix} = \begin{pmatrix} E^R_1 \\ \vdots \\ E^R_m \\ \vdots \\ E^R_M \end{pmatrix}, \tag{4}$$

where the coefficients q_{mn} are nonzero only along the diagonals and zero everywhere else.

The matrix system (4) can now be solved for the unknowns E_n. Note that the system has more equations than unknowns ($M>N$). In fact, each extra pixel of keystone gives one extra equation. For the ideal case when there is no noise in the system, the matrix system is compatible, i.e., can be solved. However, for a real system with noise, the system is overdetermined and an optimization method, such as for instance the least squares method, could be used to obtain the solution.

Simulations have shown that the restoring process (i.e., the solving of the overdetermined matrix system (3)) amplifies somewhat the noise that is present in the sensor pixels [7]. In order to limit noise amplification, while at the same time preserving spatial resolution, we recommend to have about 10% more sensor pixels than scene pixels, i.e., that M/N~1.1. In

#185751 - $15.00 USD Received 21 Feb 2013; revised 22 Apr 2013; accepted 23 Apr 2013; published 29 Apr 2013

this case, the noise will typically be amplified by a factor ~1.3. However, since the mixel camera can collect considerably more light than traditional cameras, in addition to being free of keystone errors, a significant improvement in signal-to-noise ratio will still be obtained (see Section 6).

The restoring process described in this section can be repeated for all spectral channels. This means that even though the images of the slit on the sensor have different lengths (i.e., different keystone) for different spectral channels, they will all be converted to the same final grid without introducing any blur or misregistration errors to the data. Note that the data restoring method described in this section is fundamentally different from resampling. Resampling would, if used to convert all the spectral channels to the same grid, introduce noticeable misregistration errors and blur to the data, even in the absence of noise and other error sources [8]. The suggested data restoring method, on the other hand, restores the exact scene pixel values for all spectral channels, if the light distribution over each scene pixel is uniform and if there is no noise or other error sources present in the system.

3. The light mixing chambers

The data restoring method described in the previous section requires that the intensity distribution over each scene pixel is known so that the matrix coefficients q_{mn} can be determined. This can be obtained by inserting an array of light mixing chambers into the camera slit. The purpose of the chambers is to mix the light that goes through each chamber as evenly as possible, so that the light distribution at the output of the chamber is independent of the light distribution at the input. The light distribution at the output of each chamber will then always be the same and therefore always known. Each mixing chamber is a miniaturized version of a light-pipe homogenizer [9], which in this case is optimized to provide best possible mixing for a particular numerical aperture (F-number) of the incoming light while minimizing the number of reflections. Other types of light mixing devices could possibly also be used.

The light content of each chamber corresponds to the light content of a scene pixel. The projection of a scene pixel onto the slit, as it appears after passing through the mixing chamber, will hereafter be referred to as a 'mixel'. The light content of a mixel will then be equal to the light content of the corresponding chamber and scene pixel. Since there are fewer mixels than sensor pixels, and the light distribution inside each mixel is known, it will be possible to restore the energy content of each mixel based on the recorded sensor pixel values, ref. Equation (3).

The array of light mixing chambers for such a system will typically have feature sizes in the tens of microns range for the most common wavelengths and pixel sizes. Machining tolerances will therefore be stringent. One possible method to manufacture the chambers is by use of a high-aspect-ratio micromachining technique that uses deep X-ray lithography, such as the LIGA-process [10]. Figure 6 shows an example of how the light mixing chambers may look (only a few chambers are shown), and how they alter the input signal to a form suitable for applying the restoring method. Note that light mixing takes place only inside each mixing chamber, i.e., no crosstalk between adjacent chambers is introduced at this stage.

Geometric ray tracing has been used to model the light propagation in the chambers (if the width of a spectral channel is very narrow so that the light becomes quite coherent, or if the size of the airy disk is comparable to the chamber size, then wave optics should be used instead). Many rays (a few hundred) are launched from five areas of the front face in each chamber. The density of the rays corresponds to the illumination of the corresponding area of the front face. For the calculations it was assumed that the walls of the chambers are infinitely thin and 100% reflective. In reality, the walls will have finite thickness, and some losses due to absorption and scattering must be expected. It is beneficial to have the walls significantly thinner than the width of the chambers, in order to maximize light transmission. While the presence of walls does not affect the restoring process, details of the scene may become obscured if the walls are too thick.

#185751 - $15.00 USD Received 21 Feb 2013; revised 22 Apr 2013; accepted 23 Apr 2013; published 29 Apr 2013

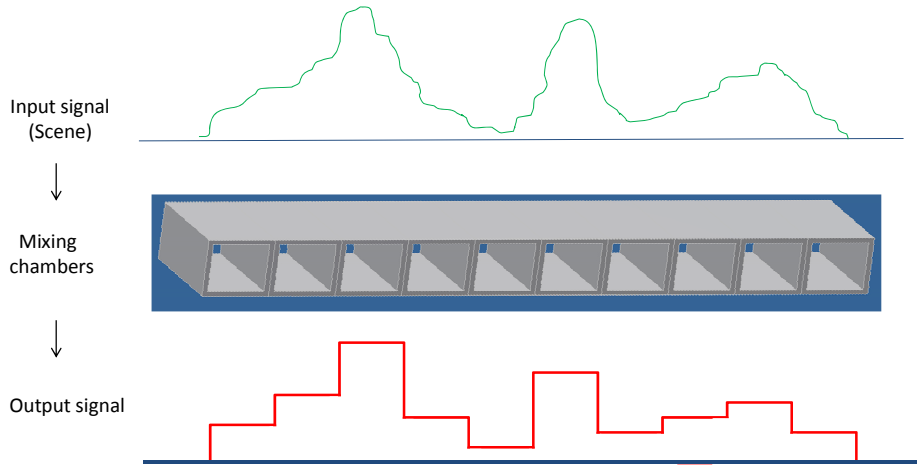

Fig. 6. The light mixing chambers. The light from the scene (green curve) is mixed in the chambers so that the light distribution at the output of each chamber (red curve) is as uniform as possible. The key is to obtain a known light distribution at the output that is independent of the light distribution at the input of the chambers. The picture of the chambers is for illustration purposes only. The dimensions of the real chambers will depend on the sensor pixel size and the optics.

Figure 7 shows how the rays are distributed inside one chamber (fewer rays are shown than what was used in the calculations). The horizontal black line shows the back face of the chamber. Choosing the right length for the chamber is crucial to obtain the best possible performance. The length (L) of the mixing chamber can be written as:

$$L = k \cdot F \cdot w \,, \tag{5}$$

where w is the width of the chamber, F is the F-number of the foreoptics, and k is a constant that is chosen in such a way that the back face of each chamber has as uniform illumination as possible. For a given k, the mixing result at the backface of a chamber with length L will be the same for any choice of F-number and width (w). We have used the value $k = 2$ in our simulations, which gives a very uniform light distribution while at the same time keeping the number of reflections as low as possible (half of the rays are reflected once, while the rest of the rays pass through the chamber without being reflected).

Figures 7(b)-7(d) show the distribution of light when the rays are launched from a single area at the front face of the chamber, simulating that light is coming only to one part of the chamber. We see that even in these extreme cases the light is mixed well. In order to preserve good light mixing, it is important to focus the foreoptics reasonably precisely on the front face of the mixing chambers, preferably to within 5% of the length of the chambers.

Figure 8 shows the performance of the light mixing chambers for a part of the scene (mixels #244-#253) that is used for the simulations in Section 5. We see that even a very uneven light distribution (blue) at the front face of the chamber corresponding to mixel #249, results in an almost completely even light distribution (red) at the back face of the chamber.

The array with mixing chambers can be thought of as a hardware sampler, where each individual chamber samples the incoming signal in the same way for different wavelengths. The data restoring method, described in Section 2, allows to reconstruct those individual samples in a lossless way for each spectral channel, based on the sensor output. The spatial resolution of the mixel camera is therefore equivalent to that of a traditional camera (where keystone is corrected in hardware) which uses the same number of pixels as there is number of mixels. However, while a traditional camera introduces misregistration errors due to keystone and blur from the relay optics into the final data cube, this is not the case for the mixel camera. The modular transfer function (MTF) of the mixel camera at the sampling frequency will therefore be determined only by the foreoptics.

#185751 - $15.00 USD Received 21 Feb 2013; revised 22 Apr 2013; accepted 23 Apr 2013; published 29 Apr 2013

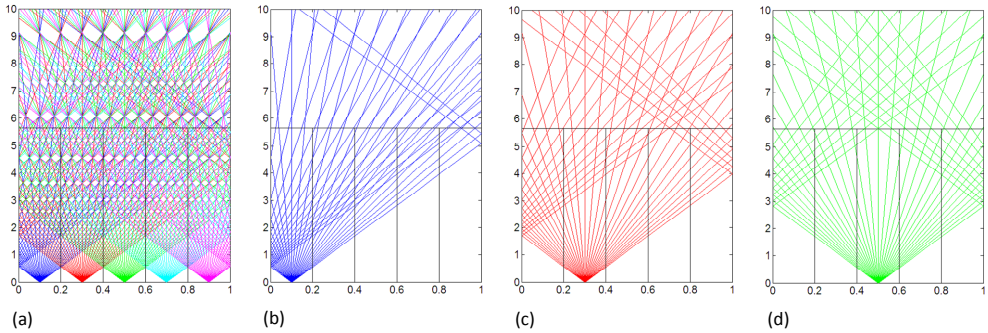

Fig. 7. Distribution of rays within a light mixing chamber. In this example, the F-number is F2.8 and the width of the chamber (x-axis) is 1. The corresponding length of the chamber (y-axis) is 5.6, as calculated from Eq. (5) with $k = 2$. The backface of the chamber is marked by a horizontal black line (approximately at the middle of the figure). (a) Rays are launched from all five areas on the front surface (bottom horizontal line). (b)-(d) Rays are launched from different single areas on the front surface. Note the different scales on the x- and y-axes. The aperture angle (10° in this example) therefore appears larger than it actually is.

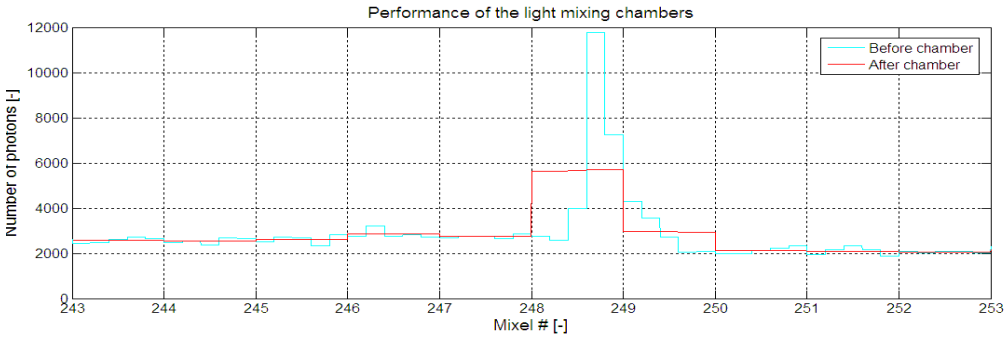

Fig. 8. Performance of the light mixing chambers.

4. Optical design

In traditional cameras, keystone (even as small as 0.1 of a pixel) introduces noticeable errors in the hyperspectral data, as we will show in Section 6.1. Keeping the keystone at such low level in a high resolution camera is extremely difficult. Design and manufacturing of the camera becomes even more difficult in the case of fast optics. For the proposed mixel camera, however, keystone correction is not required in the optics between the mixel array and the sensor. This makes it possible to design sharper optics that at the same time can collect more light, i.e., has lower F-number. Let us examine how good the optics of the mixel camera can be.

The optics of the mixel camera can be split into two parts: the foreoptics which creates an image of the scene on the mixing chambers, and the relay system which projects the slit with the mixing chambers onto the sensor. The exit plane of the mixing chambers forms the object plane for the relay system.

Figure 9 shows an example of a possible relay system for the mixel camera. This is a lens relay with magnification –0.33x. It is designed for the wave length range 420 nm-1000 nm. The relay system is telecentric both in object space and image space. The dispersive element is a diffraction grating which is placed at the aperture stop. Placing the aperture stop in the middle of the system allows for very good aberration correction. The F-number in the image plane is as low as F1.25. This is considerably lower than for the widely used Offner relay (traditionally used in hyperspectral cameras when high spatial resolution in combination with low keystone is required) which is more or less limited to F2.8 [11]. Another high-

#185751 - $15.00 USD Received 21 Feb 2013; revised 22 Apr 2013; accepted 23 Apr 2013; published 29 Apr 2013

performance camera, the HySpex VNIR1600 [12], collects slightly more light than the Offner design, with its F2.5 lens. The relay optics of the mixel camera therefore collects four times more light than most traditional high-resolution systems. The image quality is also good: this optics is suitable for a sensor with ~3000 spatial pixels.

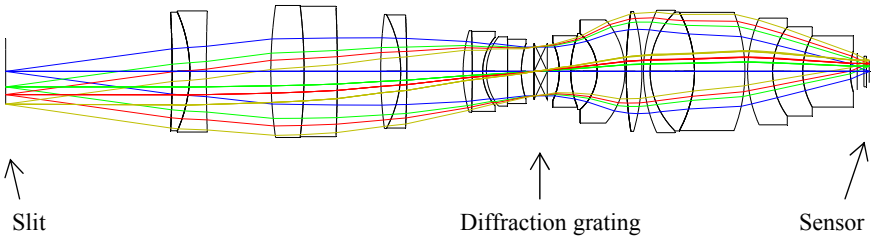

Fig. 9. An example of a possible relay system for the mixel camera. The slit with the mixing chambers is shown to the left in the figure. Different colors correspond to different field points. The direction of the dispersion is perpendicular to the drawing plane. The dispersion is therefore not visible in this figure.

The point-spread-function (PSF) of the relay optics varies a lot across the spectral channels. However, this variation will be taken into account during the restoring process (see Section 6.4). Since the PSFs can be allowed to be different, the designer can focus on optimizing the optical system for maximum sharpness and the lowest F-number.

The relay system has relatively tight centration requirements of 5-20 µm. This suggests a need for active centration, but the requirements are very well within the manufacturing capabilities of several optical companies. The part of the optics after the diffraction grating is tilted by a few degrees. Tolerances for that tilt are, however, much more relaxed than for the rest of the system and easily achievable during manufacturing.

An attractive property of the design presented here is that, unlike Offner and Dyson relays, it has a magnification which is significantly different from –1. This relay was designed to have –0.33x magnification, which means two things. First, the mixels will be much larger than the sensor pixels. If the sensor pixels are 6.5 µm, then the mixels will be approximately 3.3 times larger (assuming M/N = 1.1, see Section 2), i.e., the mixels will be approximately 21.5 µm in size. Second, the F-number for the foreoptics will be much higher than the F1.25 from the system's specifications. The foreoptics for this relay should have F-number F3.8 (= F1.25/0.33), which makes the optimum length of the mixing chambers equal to 163.4 µm, see Eq. (5). This is great news: larger mixing chambers are probably easier to manufacture, and the F3.8 foreoptics is definitely much easier to design, manufacture and align than an F1.25 one.

The requirements for the foreoptics are different than for the relay system since the restoring process restores the mixels, i.e., the scene pixel values as they appear *after* having passed through the mixing chambers in the slit. Any misregistration errors that are introduced *before* the slit will not be corrected for. It is therefore important to minimize the misregistration errors in the foreoptics. We have obtained this by using only reflective optics. In this case, the rays of all wavelengths follow precisely the same optical path and keystone cannot occur. In the relay optics, however, this is not possible since rays of different wavelengths are supposed to end up on different parts of the sensor. The rays must therefore follow different optical paths through the relay system (this is obtained by use of a dispersive element), inevitably introducing a certain amount of keystone.

Figure 10 shows an example of a possible foreoptics for the mixel camera with F3.8 and 25 degrees field of view. The foreoptics consists of three mirrors, two of them are off-axis 6th order aspheres. The centration tolerances for the mirrors are ~50 µm. The spot size is quite small compared to the mixel size. However, the PSF is slightly wavelength dependent due to diffraction. This may cause keystone-like misregistration errors in the image projected onto the slit. The F-number and mixel size are, however, chosen in such a way that the Airy disks

#185751 - $15.00 USD Received 21 Feb 2013; revised 22 Apr 2013; accepted 23 Apr 2013; published 29 Apr 2013

are quite small compared to the mixel size. The probability that this type of misregistration error occurs, as well as the value of such an error, is therefore quite low and noticeably smaller than in traditional designs. Also, it might be possible to design a refractive component to be placed right in front of the mixing chambers, which would blur the shorter wavelengths somewhat in order to equalize the PSFs for different wavelengths.

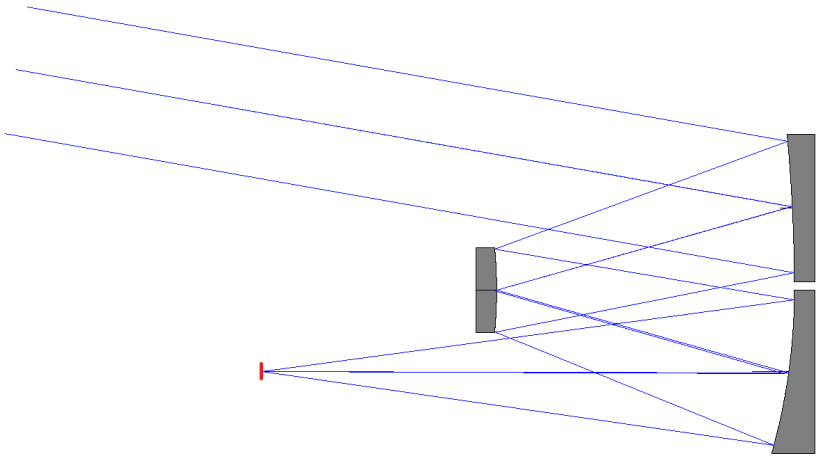

Fig. 10. Example of a possible foreoptics for the mixel camera. The location of the mixel array in the image plane is marked with red color. The direction of the mixel array is perpendicular to the figure plane.

Recently, a high performance camera design based on the Dyson relay has been proposed with F1.2 optics and less than 0.1 pixel keystone when used with a 2000 pixels sensor [13]. These are very impressive specifications for a hardware corrected camera. However, while the Dyson relay itself is keystone-free, the manufacturing tolerances are likely to cause some degree of keystone in a real system (for instance, a tilt of the spherical surface of the refractive component in the relay will introduce approximately 0.01 pixel keystone per 1 μm tilt). Also, unlike the proposed mixel camera optics, the Dyson relay imposes very high requirements on the foreoptics, which in this case has to be F1.2 and to resolve 2000 spatial elements. This limits the design choices. The Schmidt foreoptics proposed by the authors is suitable for a narrow field of view of 4 degrees, but may be difficult to use for wider angles, as it already introduces ~0.1 pixel keystone at the edges of the field of view according to the authors. The optics is designed for the sensor to be positioned directly on a flat optical surface of the refractive component in the Dyson relay, and the sensor should be placed relatively close to the slit. This limits the choice of sensor. Nevertheless, the proposed Dyson system with Schmidt foreoptics offers a high level of performance, despite these drawbacks. The example design of the mixel camera does not have an advantage in terms of light gathering capacity in this case. However, the mixel camera concept is much more flexible in its ability to customize the field of view and promises much lower keystone errors for a significantly higher pixel count. It is also relatively straightforward to manufacture and assemble.

The optics of the mixel camera presented in this section is merely a starting point, but shows how easy it is to design a high performance hyperspectral imager using the mixel camera concept. The lens relay presented here is larger than Offner and Dyson relays, as we were focusing on achieving high spatial resolution (by hyperspectral standards), low F-number, and ease of manufacturing. The optics can be further customized or improved. The field of view of the foreoptics can be changed and increased to at least 40 degrees. If the magnification of the relay is changed from −0.33x to −0.16x, for example, then the required F-number for the foreoptics will increase to F7.5. This will allow for an even wider field of view and even more relaxed centration tolerances for the mirrors. The relay optics can be modified in order to improve spatial resolution (for a sensor with significantly higher pixel

#185751 - $15.00 USD Received 21 Feb 2013; revised 22 Apr 2013; accepted 23 Apr 2013; published 29 Apr 2013

count) and/or F-number in the image space. The wavelength range can also be expanded to 400 nm. Alternatively, a completely different layout can be adopted, for example, with focus on smaller size or expanded wavelength range instead of highest possible spatial resolution and light throughput.

An optical designer will always have more flexibility when thorough aberration correction on subpixel level is no longer required. This flexibility, provided by the mixel camera concept, should allow to push camera specifications beyond what is currently possible. However, even in its present state the suggested optics for the mixel camera seems to meet or exceed the specifications of the best available high-resolution hyperspectral cameras.

5. Virtual camera simulations

In order to evaluate and compare the performance of the mixel camera to traditional hyperspectral cameras where the keystone has been corrected in hardware (HW corrected cameras), a Virtual Camera software was developed [14]. The Virtual Camera software simulates the performance of a hyperspectral camera and uses the hyperspectral data of a real scene (captured by a real hyperspectral camera) as input. The virtual camera distorts the input data somewhat in accordance with the modeled optical distortions, sensor characteristics, and photon noise. Then by comparing the data at the output of the virtual camera with the data at the input, we are able to evaluate the performance of the camera.

A hyperspectral data set containing 1600 spatial pixels, originally captured using a HySpex VNIR1600 hyperspectral camera [12], forms the "continuous" 1-dimensional scene (blue curve in Fig. 11) to be captured by the virtual camera. The virtual camera is set to have significantly lower resolution (320 pixels) than the resolution of the scene. This means that 5 spatial pixels from the HySpex VNIR1600 data set form 1 scene pixel. By doing this, we simulate the fact that any real scene contains smaller details than the resolution of the camera being tested.

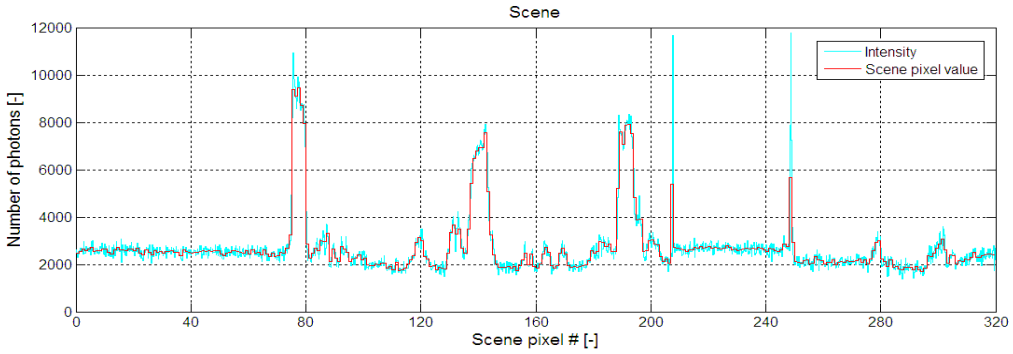

Fig. 11. The reference scene consisting of 320 scene pixels. The blue curve shows the photon number density, while the corresponding scene pixel values are shown in red.

Figure 11 shows the number of photons in the signal from the scene for one spectral band. The signal contains large areas with slowly changing brightness, relatively sharp borders between such areas, and some quite small objects which are significantly different in intensity compared to the background. This scene will therefore allow us to examine how the two cameras perform on different scene features. Further, the number of pixels is large enough that some conclusions can be drawn based on statistics.

Both photon and readout noise are included in the simulations. The readout noise depends on the choice of sensor. One of the best available sensors [15], which we will use as a reference, has the following specifications: full-well is 30 000 electrons and the readout noise in the global shutter mode is 3 electrons (rms) with Gaussian distribution. In order to meet the requirements for pixel full-well, typically 2 or 3 pixels will be binned in the spectral direction (perpendicular to the direction of the slit), giving a full-well of up to 90 000 electrons and readout noise of about 5 electrons. We see that the input signal (Fig. 11) is well below

#185751 - $15.00 USD Received 21 Feb 2013; revised 22 Apr 2013; accepted 23 Apr 2013; published 29 Apr 2013

saturation. For the calculations, we will assume that the quantum efficiency is 100%, i.e., when 1 photon is hitting the sensor 1 electron-hole pair is being generated.

When photon noise is included, the number of photons in the signal follows a Poisson distribution with mean E and standard deviation $\sqrt{E}$ [16]. Here E is the number of photons in the noise-free signal. The resulting relative error in the signal due to photon noise has zero mean value and standard deviation:

$$\sigma = \frac{1}{\sqrt{E}}. \tag{6}$$

The relative error due to photon noise decreases when the signal increases. When the signal increases by a factor 2 the relative error decreases with a factor $\sqrt{2}$. Figure 12 shows the relative error (1σ) as a function of number of photons in the signal.

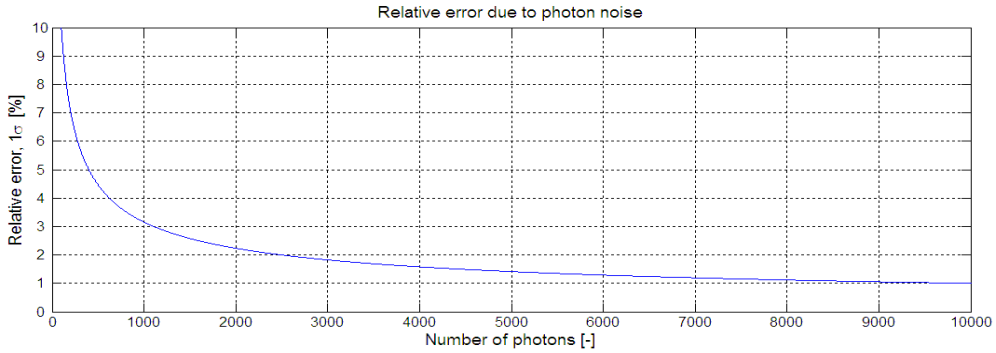

Fig. 12. Relative error (1σ) due to photon noise as a function of the number of photons in the signal.

When evaluating the performance of the cameras, we calculate the error in the final data relative to the input. The relative error, dE, is given by:

$$dE = \frac{(E_{final} - E_{init})}{E_{init}}, \tag{7}$$

where E_{init} is the scene pixel value (number of photons) and E_{final} is the calculated value of the same scene pixel after the signal has been processed by the camera. We can then find the standard deviation of dE over the 320 pixels and we can also determine the maximum relative error. Both are important parameters when evaluating the performance of the cameras.

6. Camera performance

The best hyperspectral cameras on the market are specified to have less than 0.1 pixel keystone. The performance of the mixel camera will therefore be compared to a HW corrected camera with 0.1 pixel keystone. In reality, however, the keystone is often 0.3 pixel or more for many cameras. We will therefore also compare the mixel camera to a HW corrected camera with 0.3 pixel keystone. The mixel camera has 32 pixels keystone, i.e., the 320 scene pixels (or mixels) are recorded onto 352 sensor pixels. The mixel camera is also able to collect about four times more light than traditional high-resolution cameras (see Section 4) and this will be taken into account in the analyses.

If resampling of the data in postprocessing is considered acceptable, the misregistration errors of a HW corrected camera with a certain residual keystone could in principle be somewhat reduced. However, the keystone stability of such cameras is of concern. Alternatively, resampling could be used in a camera with uncorrected keystone. Such a resampling camera would have the same advantages as the mixel camera with respect to light gathering capacity and high spatial resolution, but the misregistration errors would be

#185751 - $15.00 USD Received 21 Feb 2013; revised 22 Apr 2013; accepted 23 Apr 2013; published 29 Apr 2013

equivalent to those of a HW corrected camera with 0.1 pixel keystone. The performance of such a resampling camera is discussed in [8], and compared to the mixel camera in [14]. Here we will focus the discussion on mixel camera performance compared to cameras with well-corrected keystone that do not use resampling.

In Section 6.1 we look at misregistration errors alone, before moving on to investigate what happens when photon and readout noise are present in the system in Section 6.2. Section 6.3 treats the bright light case, which truly highlights the benefits of the mixel camera compared to traditional HW corrected cameras. Then, in Section 6.4, we show how to handle variations in PSF across different wavelengths and the potential errors connected to this. Finally, in Section 6.5 we look at the errors resulting from misalignment between the mixel array and the sensor pixels, demonstrating the need for a very precise calibration of the system. The scene in Fig. 11 is used as the input signal for all the calculations in this section.

6.1 Misregistration errors

In this section we compare the misregistration errors from a mixel camera to the misregistration errors from a HW corrected camera with 0.1 pixel keystone. Photon and readout noise are not included in the calculations. Figure 13(a) shows the misregistration errors for the HW corrected camera. The graph shows random looking errors with standard deviation 1.9% and distinct peaks up to 15% in the areas with large differences between adjacent pixels.

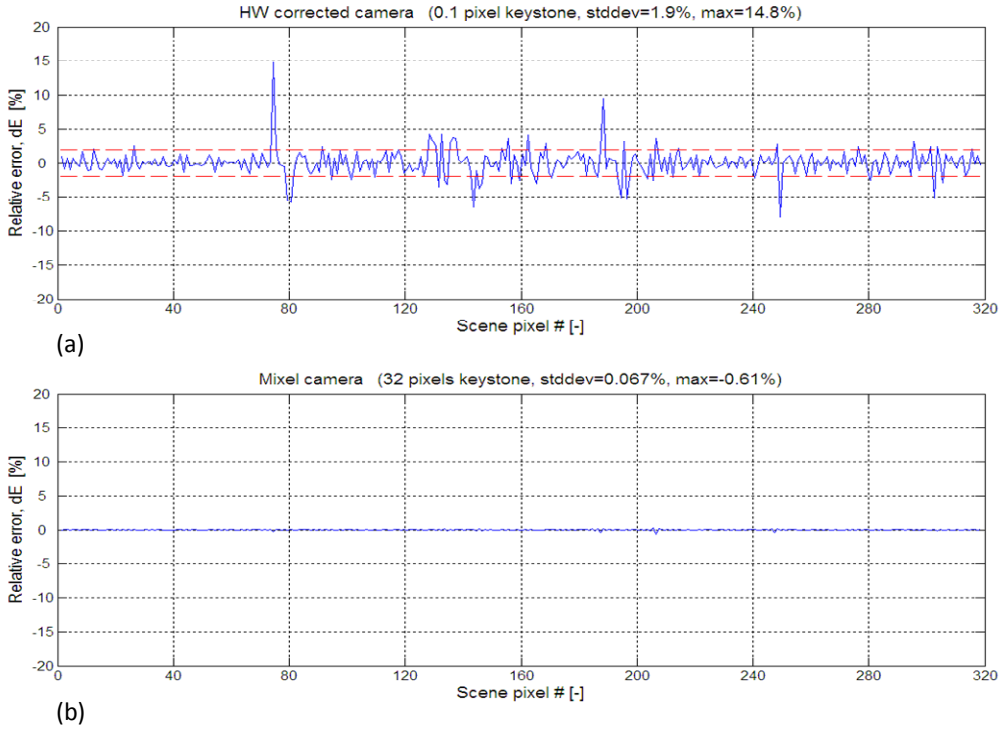

Fig. 13. Misregistration errors for (a) the HW corrected camera with 0.1 pixel keystone and (b) the mixel camera. The standard deviation of the error is marked by a dashed red line. Photon and readout noise are not included.

Figure 13(b) shows the misregistration errors for the mixel camera. These errors are due to the fact that the mixing chambers do not mix the light perfectly (see Section 3). Compared to the results for the HW corrected camera, this looks very promising. The misregistration error is practically zero with standard deviation 0.07% and peaks up to only 0.6%.

#185751 - $15.00 USD Received 21 Feb 2013; revised 22 Apr 2013; accepted 23 Apr 2013; published 29 Apr 2013

6.2 Errors when photon and readout noise are included

We will now look at what happens to the errors when photon and readout noise are included. Figure 14(a) shows the results for a HW corrected camera with 0.1 pixel keystone. The standard deviation of the relative error has increased from 1.9% to 2.8%, but the peaks are similar to before (Fig. 13(a)). It looks like the photon and readout noise are not able to completely mask the misregistration errors at this signal level.

Figure 14(b) shows the results for a HW corrected camera with 0.3 pixel keystone. The standard deviation of the relative error has now increased to 5.8% and the maximum error is as large as 48%. Clearly, the presence of 0.3 pixel keystone in the system has a large impact on the data quality.

Figure 14(c) shows the results for a mixel camera that collects the same amount of light as the HW corrected cameras. We see that the mixel camera has similar performance to the HW corrected camera with 0.1 pixel keystone (standard deviation 2.7% versus 2.8% and peaks up to 13% versus 16%). We expected the errors to be somewhat larger for the mixel camera in this case due to noise amplification (see Section 2), but the almost complete absence of misregistration errors seems to outweigh this effect.

However, the mixel camera is capable of collecting about four times more light than the HW corrected cameras. Figure 14(d) shows the relative error in this case. The difference in performance is now very visible, when compared to the HW corrected camera with 0.1 pixel keystone: standard deviation 1.4% versus 2.8% and peaks less than 5% versus almost 16%. Unlike the graphs for the HW corrected systems (Figs. 14(a) and 14(b)), the graphs for the mixel cameras (Figs. 14(c) and 14(d)) do not contain any large peaks connected to scene features. The misregistration error of a mixel camera is virtually zero (Fig. 13(b)), and the performance of the mixel camera is therefore limited only by photon noise. More light – better performance (as we will see in the next section), and no peaks in the areas with large differences between adjacent pixels.

6.3 Bright light

We will now look at the camera performance in bright light conditions. Imagine that the amount of light in the scene is so large that the sensor pixels of the HW corrected camera are almost saturated. The integration time for the mixel camera (that collects four times more light) must then be shortened in order not to saturate the sensor. How does the mixel camera perform compared to the HW corrected camera when they both receive the same amount of light under optimum light conditions?

When the HW corrected camera with 0.1 pixel keystone (Fig. 15(a)) is receiving five times more light than in the previous examples, the standard deviation of the relative error decreases from 2.8% to 2.1%. However, the peak error remains more or less the same (around 15%).

The mixel camera (Fig. 15(b)) shows much better performance under the same light conditions. The standard deviation of the error is 1.3%. The maximum error is only about 4% and not linked to any signal features. The errors are dominated by photon noise and appear completely random.

In principle, it may be possible to avoid saturation in the mixel camera by either using multiple exposures (provided that the sensor is fast enough) or by increasing the dispersion in the camera and binning eight pixels in the spectral direction, giving a full-well of 240 000 electrons. The mixel camera can then again collect four times more light.

Figure 15(c) shows the relative error of such a mixel camera. The errors are now remarkably low (standard deviation 0.6% and maximum error less than 2%) and still appear completely random. Even in so bright light the performance of the mixel camera is limited only by photon noise!

#185751 - $15.00 USD Received 21 Feb 2013; revised 22 Apr 2013; accepted 23 Apr 2013; published 29 Apr 2013

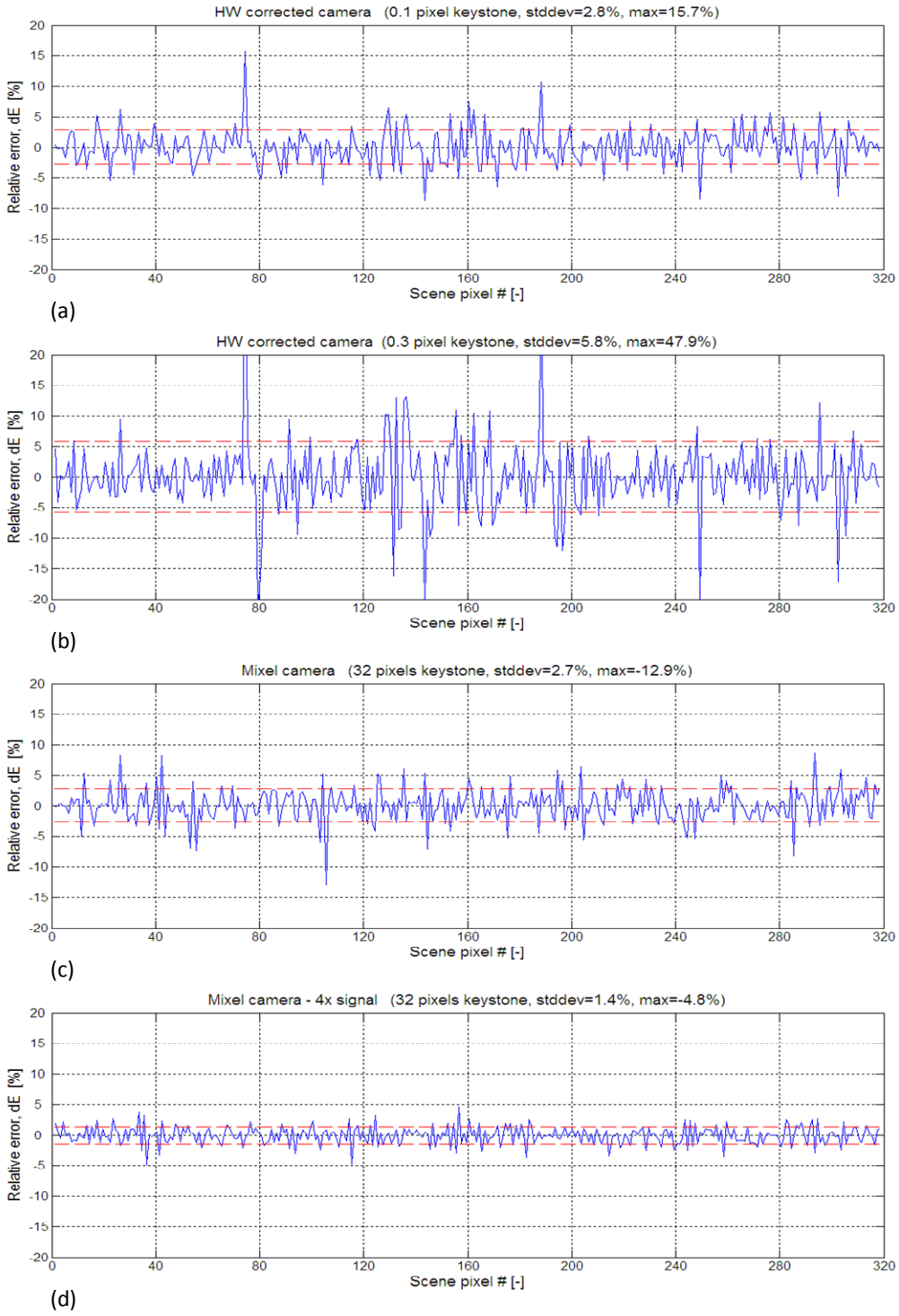

Fig. 14. Camera performance when photon and readout noise are included. The figures show the relative error for (a) a HW corrected camera with 0.1 pixel keystone, (b) a HW corrected camera with 0.3 pixel keystone, (c) a mixel camera that collects the same amount of light as the HW corrected cameras and (d) a mixel camera that collects four times more light. The standard deviation of the error is marked by a dashed red line.

#185751 - $15.00 USD Received 21 Feb 2013; revised 22 Apr 2013; accepted 23 Apr 2013; published 29 Apr 2013

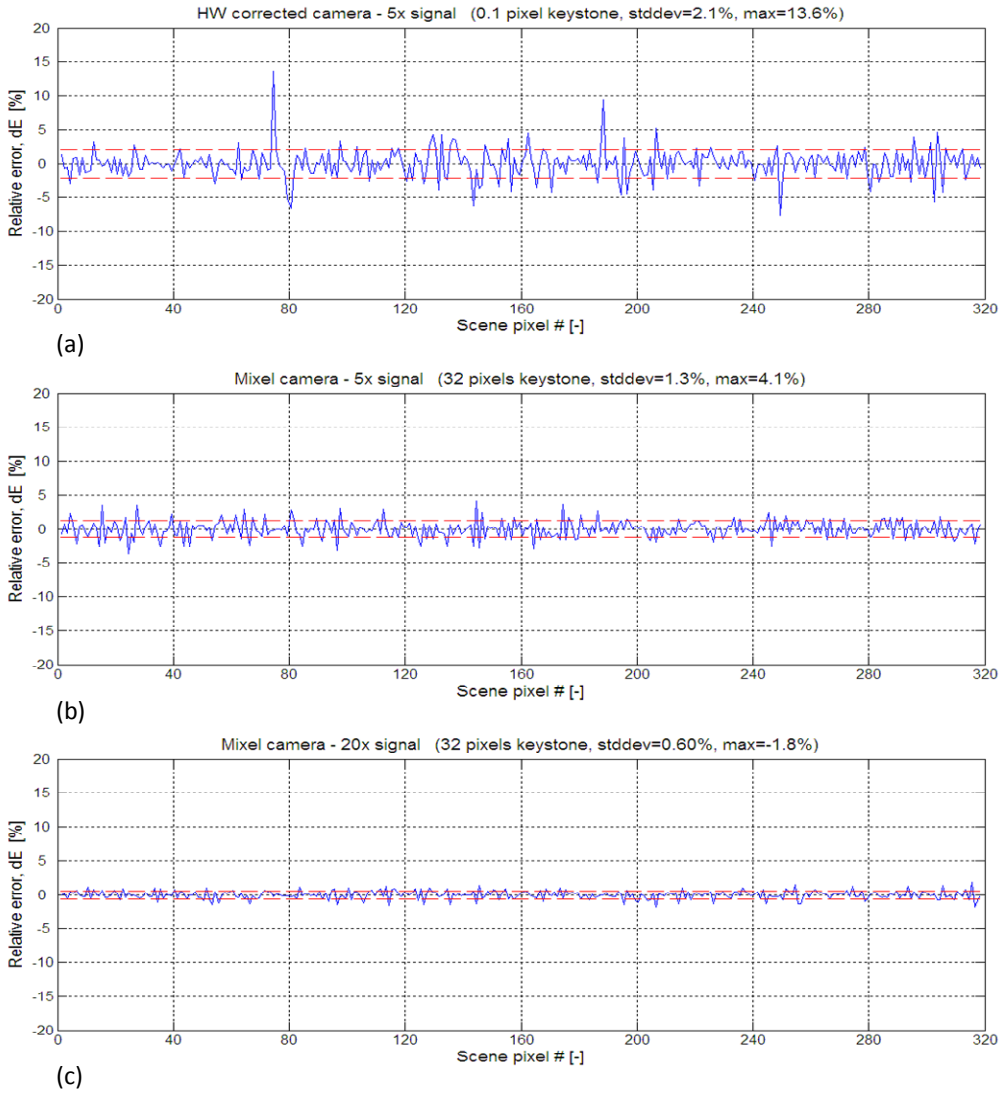

Fig. 15. Camera performance in bright light when photon and readout noise are included. (a) Relative error for a HW corrected camera with 0.1 pixel keystone, (b) relative error for a mixel camera that collects the same amount of light as the HW corrected camera and (c) relative error for a mixel camera that collects four times more light. The standard deviation of the error is marked by a dashed red line.

6.4 Transitions between mixels

So far, we have assumed that the transitions between the mixels in the mixel camera are instant. In a real camera, the signal is blurred in the optics between the slit and the sensor, so that the transitions between the mixels are no longer instant when the mixels are projected onto the sensor. However, if the shape of the transition is known, the mixel content can be accurately restored as before. Note that it is the initial "sharp" data (where the transitions are instant) that are being restored, i.e., we restore the mixel content as it was before being blurred in the relay optics. If the shape of the transition is not known, or is known only approximately, errors will be introduced in the restored signal.

In order to investigate the magnitude of these errors, we simulate a system with given transitions between the mixels and try to restore the data while making different assumptions

#185751 - $15.00 USD Received 21 Feb 2013; revised 22 Apr 2013; accepted 23 Apr 2013; published 29 Apr 2013

about the transitions. For these simulations we have assumed that the mixing of the light in the mixing chambers is perfect (as opposed to the simulations in the previous sections where geometric ray tracing was used to model the light mixing) and that there is no noise in the system. Any errors in the restored signal will then be due only to the discrepancy between the *actual* transitions and the *assumed* transitions in the system.

We have used third order polynomials to model the transitions. In reality the transitions will not look exactly like this, but it will be sufficient to give us a good indication of the errors involved. Figure 16 shows an example of a third order polynomial transition (red) between two mixels. The transition starts at $x = x_1$ and ends at $x = x_2$. The 'sharp' value of mixel #1 (i.e., the signal level of the part of the mixel that is not affected by the transition) is equal to E_1. The 'sharp' value of mixel #2 is equal to E_2.

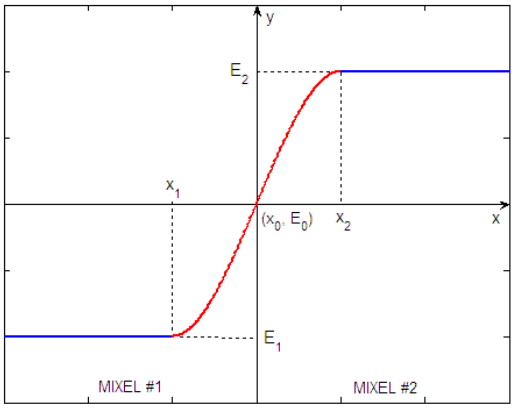

Fig. 16. Example of a third order polynomial transition (red).

The equation for the third order polynomial transition is:

$$y = a(x - x_0)^3 + c(x - x_0) + E_0, \tag{8}$$

where a and c are two constants:

$$\begin{aligned} a &= -\frac{4c}{3(x_2 - x_1)^2}, \\ c &= \frac{3(E_2 - E_1)}{2(x_2 - x_1)}. \end{aligned} \tag{9}$$

The transition has odd symmetry about its center (x_0, E_0), with $x_0 = (x_1 + x_2)/2$ and $E_0 = (E_1 + E_2)/2$. In order to calculate the transition between the two mixels, we must know the width and position of the transition zone, i.e., x_1 and x_2, and the 'sharp' mixel values E_1 and E_2. A transition that extends 30% into each mixel is here referred to as a 30% transition.

The width of the transition will in general be wavelength and field dependant. Imagine that in the real system we only know the transition for a wavelength somewhere at the middle of the spectrum. We use this value also for all the other wavelengths when we restore the mixel values, but let us say that in this particular system the shorter wavelengths will have a somewhat narrower transition than what we are assuming and the longer wavelengths will have a somewhat wider transition. How will this affect the errors in the restored data?

This situation was investigated by simulating four cases where the true transitions are 20%, 30%, 40%, and 50% respectively and then restoring the data *assuming* 35% transitions in each case. Figure 17 shows the resulting errors when the transitions are 50% and 40% (cases with 20% and 30% transitions have similar errors with opposite sign). We see that we get the largest errors when the deviation between the assumed transitions (35%) and the true transitions (50%) is the largest, see Fig. 17(a). The standard deviation is small (0.7%) but the

#185751 - $15.00 USD Received 21 Feb 2013; revised 22 Apr 2013; accepted 23 Apr 2013; published 29 Apr 2013

peaks are quite large (up to about 6%). When the deviation is smaller (when the true transitions are 40%), the standard deviation decreases to about 0.2% and the largest peaks are only about 2%, see Fig. 17(b).

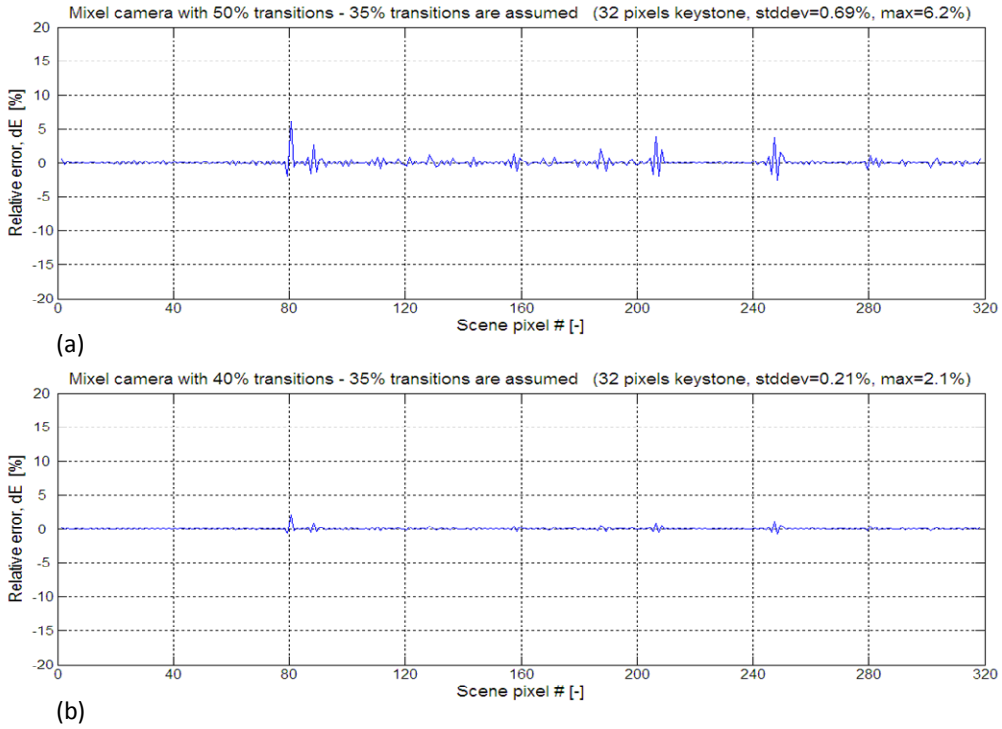

Fig. 17. Mixel camera with (a) 50% transitions and (b) 40% transitions. The data are restored assuming 35% transitions. Photon and readout noise are not included.

The results in this section show that the presence of transitions does not prevent us from restoring the data, but that it is important to know the shape of the transitions reasonably well. We expect that in a real system the point spread function will be accurately measured for several wavelengths at several field points, providing the necessary information about the transitions. Alternatively, we can assume a certain transition that is not too much off, and restore the data according to this assumption. This will eliminate the hazzle of determining the shape of the actual transitions, and the resulting error may still be acceptable.

6.5 Misalignment in the relative position between the mixel array and the sensor pixels

So far, we have assumed that the relative position of the mixel array and the sensor pixels in the direction along the mixel array is known with absolute accuracy. In reality, there will be errors in the determination of the relative position (misalignment) and this will lead to errors in the restored data. We have investigated how large these errors will be. For the calculations we have assumed that the signal is perfectly mixed in the mixing chambers and that there are no other error sources present. The transitions between the mixels have been modeled as being instant.

Figure 18(a) shows the resulting error in the restored data when the misalignment between the mixel array and the sensor pixels is 0.06 pixel. We see that the error is comparable to that of a HW corrected system with 0.1 pixel keystone (Fig. 13(a)). The standard deviation of the errors is 2% (versus 1.9%) with peaks up to about 18% (versus 15%).

Figure 18(b) shows the resulting error in the restored data when the misalignment is only 0.01 pixel. The error is now quite small with standard deviation 0.3% and peaks up to 3%. We have also calculated the error when the misalignment is as small as 0.001 pixel (not

#185751 - $15.00 USD Received 21 Feb 2013; revised 22 Apr 2013; accepted 23 Apr 2013; published 29 Apr 2013

shown here). The error is then very small with standard deviation 0.03% and peaks up to 0.3%, and can be considered negligible.

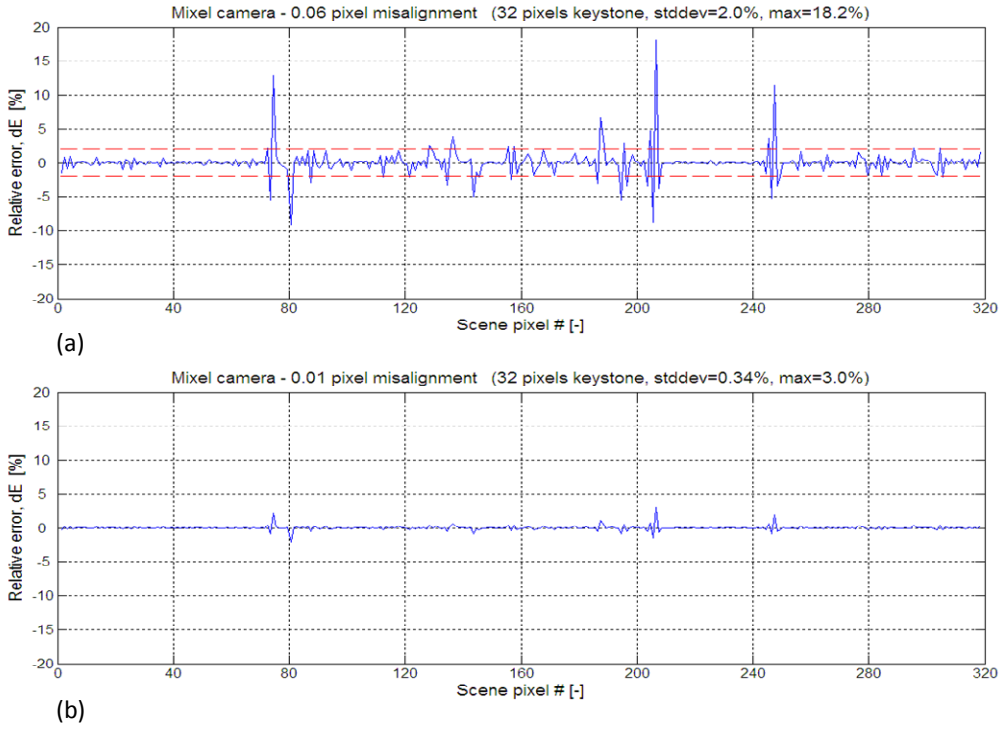

Fig. 18. Relative error for the mixel camera due to (a) 0.06 pixel and (b) 0.01 pixel misalignment between the mixel array and the sensor pixels. The standard deviation of the error is marked by a dashed red line. Photon and readout noise are not included.

We conclude that any change in the relative position between the mixel array and the sensor pixels, that is not accounted for, should be less than 0.01 pixel and preferably as small as 0.001 pixel, in order not to contribute noticeably to the errors. In the slit plane this corresponds to a required precision of ± 0.0091 mixel or better (assuming that the image of a mixel covers 1.1 sensor pixels), which for 21.5 µm large mixels translates into a precision of about ± 200 nm. In the following section we will show how to measure with high precision the relative position between the mixel array and the sensor pixels.

7. Camera calibration

Solving the overdetermined matrix system (3) will only provide correct mixel values if the coefficients q_{mn} are correct. These coefficients describe the geometry of the mixel array image on the sensor, as well as the PSF of the relay optics, and must be determined precisely.

The relative position between the mixel array and the sensor pixels can be measured by placing a single mixel at one side of the slit, see Fig. 19. The light from the single mixel will illuminate an area on the sensor somewhat larger than one pixel, see Fig. 20. The intensity distribution (blue curve) is determined by the size of the mixel and the point spread function of the relay optics. If we know the shape of the intensity distribution, we will be able to derive the relative position of that mixel and the sensor pixels since we can measure the signal from the illuminated pixels.

Mounting the slit with the mixing chambers on a high resolution translation stage, and moving it relative to the sensor, makes it possible to measure the intensity distribution from the single mixel at the end. Piezo-electric translation stages with subnanometer resolution are readily available as off-the-shelf components at relatively low cost. Such translation stages

#185751 - $15.00 USD Received 21 Feb 2013; revised 22 Apr 2013; accepted 23 Apr 2013; published 29 Apr 2013

can move with a resolution far better than the ± 200 nm requirement for the determination of the relative position between the mixel array and the sensor pixels. By reading out the signal from the illuminated pixels, then move the slit with the single mixel by a few nanometers, take another readout, move the mixel again, take another readout, etc., it will be possible to determine the intensity distribution in the sensor plane. Alternatively, the data can be stored as a look-up table for finding the position of the single mixel relative to the sensor.

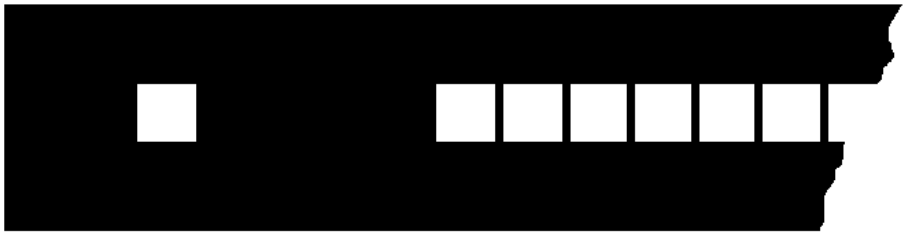

Fig. 19. The mixel array with one single mixel at the left end of the slit.

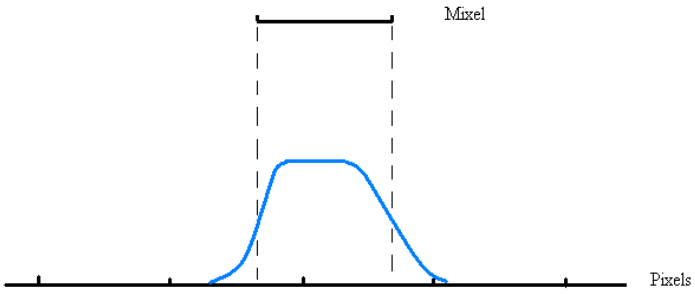

Fig. 20. Intensity distribution (blue curve) of light coming from a single mixel onto the sensor pixels. The shape of the curve is determined by the size of the mixel and the point spread function of the relay optics.

If we also place a single mixel at the other end of the slit, then we will be able to measure both the length of the slit and its position relative to the sensor. It may even be possible to do this during normal image acquisition, by using either a dedicated light source for each single mixel or even the light coming from the scene through these two mixels. This means that more or less every frame captured by the camera will have calibration data that can be used when restoring the image, i.e., requirements for alignment stability during operation will be far more relaxed (μm range instead of nm range).

Actually, extra mixels combined with a translation stage may also be a very useful tool for measuring the size and shape of the transitions between mixels, not only at the edges of the field of view but everywhere. Knowing the size and shape of the transitions is important when restoring the data (Section 6.4). If we introduce a second array of mixels which is parallel to the main array of mixels (Fig. 21), then the intensity distribution (i.e., the transitions) can be determined at several field points for all wavelengths.

During this type of calibration, the main mixel array (the upper one) is covered by a shutter and the secondary mixel array (the lower one) is used for measuring the illumination curves for many wavelengths and field points simultaneously. This calibration may be performed in a lab, or perhaps the calibration equipment may even be built into the camera. When the calibration is complete, the secondary mixel array is covered by a shutter. The main mixel array can then be used for image capture, while the single mixels on each side of the mixel array are used for real time measurements of the slit position and length.

#185751 - $15.00 USD Received 21 Feb 2013; revised 22 Apr 2013; accepted 23 Apr 2013; published 29 Apr 2013

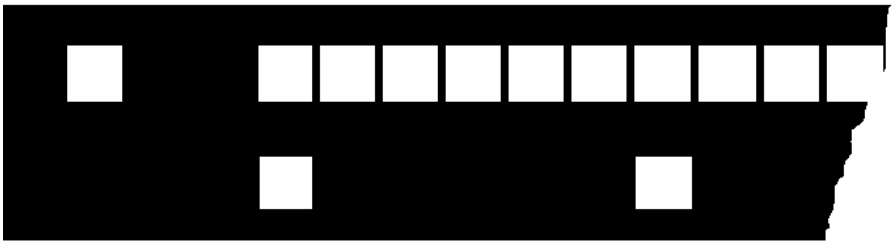

Fig. 21. The mixel array with a single mixel at the end and a second mixel array below.

8. Conclusion

The mixel camera, presented in this paper, is a new type of push-broom hyperspectral camera which has the potential to significantly outperform the existing push-broom instruments.

The fundamental advantage of the mixel camera, compared to the existing instruments, is the virtually perfect correction of the keystone and PSF variations (that are always present in the optics) in the final hyperspectral datacube. No additional blur is introduced during the conversion of the sensor data into the hyperspectral datacube; on the contrary – the blur, introduced by the relay system, is actually *removed* from the hyperspectral data.

Other potential advantages of the mixel camera are increased spatial resolution and improved signal-to-noise ratio, which come as a direct consequence of the fact that it is no longer necessary to correct keystone and PSF variations in the optics. Existing push-broom cameras have very tight requirements for keystone and PSF corrections in the optics, and this severely limits optical design in terms of achievable spatial resolution and light gathering capacity. The mixel camera is not limited by such constraints and can therefore have both significantly higher spatial resolution and increased signal-to-noise ratio compared to the existing push-broom cameras.

Many applications, such as spectral signature analysis, anomaly detection algorithms, etc., could take advantage of the technology presented in this paper. In fact, it is difficult to imagine applications which would *not* be able to benefit from a camera with practically perfect keystone and PSF corrections, high signal-to-noise ratio and very high spatial resolution.

A prototype of the mixel camera has been built and is currently being tested.

#185751 - $15.00 USD Received 21 Feb 2013; revised 22 Apr 2013; accepted 23 Apr 2013; published 29 Apr 2013